THE JOURNAL OF PHYSICAL CHEMISTRY B

B: Liquids, Chemical and Dynamical Processes in Solution, Spectroscopy in Solution

Operando XAS and UV-vis Characterization of the Photodynamic Spiropyran-Zinc Complexes

Anatoly V. Chernyshev, Alexander A. Guda, Andrea Cannizzo, Ekaterina V. Solov'eva, Nikolai A. Voloshin, Yury V. Rusalev, Viktor V. Shapovalov, Grigory Smolentsev, Alexander V. Soldatov, and Anatoly V. Metelitsa

J. Phys. Chem. B, **Just Accepted Manuscript** • DOI: 10.1021/acs.jpcb.8b11010 • Publication Date (Web): 18 Jan 2019

Operando XAS and UV-vis Characterization of the Photodynamic Spiropyran-Zinc Complexes

A.V. Chernyshev[1], A.A. Guda[2]*, A. Cannizzo[3], E.V. Solov'eva[1], N.A. Voloshin[1], Yu. Rusalev[2], V.V. Shapovalov[2], G. Smolentsev[4], A.V. Soldatov[2], A.V. Metelitsa[1]*

[1] Institute of Physical an Organic Chemistry, Southern Federal University, Stachka Ave., 194/2, 344090, Rostov-on-Don, Russia

[2] The Smart Materials Research Institute, Southern Federal University, Sladkova str. 178/24, 344090, Rostov-on-Don, Russia

[3] Institute of Applied Physics, University of Bern, Sidlerstrasse 5, 3012 Bern, Switzerland

[4] Paul Scherrer Insitute, Villigen 5232, Switzerland

ABSTRACT

Thermal and photoinduced processes accompanied complexation of photochromic spiropyrans (SPP) with Zn ions in acetone solution were characterized by means of UV-Vis and X-ray absorption spectroscopies in operando regime. SPP ligands are usually transparent at $\lambda > 350$ nm but, after mixing with Zn ions, they produce a stable colored (ε=32000-38000 $M^{-1}cm^{-1}$) complex

with maximum absorption at 525 nm that makes them a powerful tool for monitoring metal ion concentration in solution. Complex revealed fluorescence and photochromic behavior under static irradiation with visible light with constant photoreaction quantum yield across its characteristic absorption band. Zn K-edge X-ray absorption spectra show prominent changes in Zn local atomic structure between free Zn ions and Zn complex. Pump flow probe scheme was adapted to measure operando changes in Zn coordination upon light irradiation. Within experimental time resolution we have determined that after 20 μs from light irradiation Zn ion is released out of the complex. This is the first example of the direct spectroscopic probe of the Zn photorelease from the spiropyran complex.

1. Introduction

Spiropyrans (SPP) exhibit well-known photochromic reaction of photoinduced interconversion between the original colorless spiro-form (SP) and the colored merocyanine (MC) form[1-3]. Apart from differences in spectral properties, SP and MC isomers differ from each other in chemical properties towards different substrates. The merocyanine form of the spiropyran contains a negatively charged phenolate oxygen atom and readily behaves as a monodentate ligand in complexation reactions with metal ions[4-5]. Introduction of additional donor groups into the molecule structure increases the stability of such complexes. The color and fluorescence of the complexes differ from color and fluorescence of both the initial spirocyclic form and the photoinduced merocyanine isomer[6-9]. Moreover, after binding of MC with metal ions, complexes can be converted to the SP form upon irradiation with visible light upon release of the metal ions. Thus, the combination of photochromic and complexation properties opens vast perspectives for application of spiropyrans in the design of photodynamic metal ion sensors for real-time sensing

in such fields as environmental monitoring and clinical diagnostics[10-13], visualization[14-17] and tracking[18] of mobile forms of a metal ion in biological objects. In addition, it was theoretically predicted that the metal-induced isomerization of the benzothiazole-substituted spiropyran leads to switch their hyperpolarizabilities. Such a process can give rise to large contrasts of the second-order nonlinear optical properties which strongly depended on the nature of the metal ion, providing a key for selective sensing[19]. The possibility of the photoinduced structure alteration of the MC ligand being in the complex with transition metal ions will allow manipulating its magnetic properties[20] that open vast perspectives to construct photodriven magnetics. In this regard understanding the process following the photoexcitation of spiropyran-metal ion complexes is a challenge that becomes increasingly important for numerous applications in chemistry, molecular biology, and materials science. However, by the moment the photoinduced processes in excited spiropyran-metal complexes are still poorly investigated. The main experimental approaches to solve this task are based on the methods of electron absorption and emission spectroscopies including time-resolved methods and NMR spectroscopy. Chibisov and Goerner have demonstrated by means of nanosecond laser photolysis that in the case of 8-methoxy substituted spiropyran-metal complexes the deactivation processes of the excited complex are, essentially, fluorescence, intersystem crossing, trans-cis isomerization of ligand molecule or photodissociation whereas, for transition metals such as Co(II), Ni(II) or Cu(II), intramolecular energy transfer dominates[21]. Recently for *bis*(pyridinemethyl)amine substituted spiropyran complexes with yttrium and dysprosium using NMR technique it has been demonstrated that visible light irradiation of the complexes causes either irreversible decay[22] or *trans-cis* isomerization of the MC ligand without dissociation of the bond metal-phenolate oxygen atom[23], depending on the counter-ion.

In case of magnetic resonance imaging contrast agent based on complexes of gadolinium with the MC form of the spirobenzopyrans bearing tetraazamacrocyclic derivatives, irradiation induces reversible isomerization of the ligand towards the SP form. This modifies the interaction between water molecules and Gd ions changing the relaxivity[24,25].

All the mentioned above methods (i.e. UV/Vis absorption, fluorescence, relaxivity of protons etc.) are sensitive mainly to changes in electronic structure in MC ligands or reorganization of secondary (water) ligands. In addition, there are very few works focusing on the complex phototransformation in terms of metal ion coordination and properties. The only example is a work by Winkler and coworkers[26] where photoirradiation of a solution of Zn-quinoline derived SPP complex was monitored using square wave voltammetry technique. They observed rise of the free Zn^{2+} cathodic wave, confirming the ejection of metal ions from the merocyanine complex.

X-ray absorption spectroscopy is a unique tool to investigate such photo-transformations because it is sensitive to the charge state and local atomic structure around absorbing atoms[27]. Both near-edge (XANES) and extended fine structure (EXAFS) of spectra could be used to analyze local coordination around 3d metals. In the work of D'Angelo and Migliorati[28], this method allowed to distinguish between octahedral coordination of Zn^{2+} ion and Jahn-Teller distorted square-pyramidal coordination of Cu^{2+} in acetonitrile solution. Quantitative analysis of XANES spectra[29, 30] can be used subsequently to extract bond length and distortion angles[31] for the optically excited metal complexes in solution. Recent efforts in experimental techniques made XANES a versatile tool for studying photodynamical processes with the 3d metal complexes[32, 33]. In this work we apply, for the first time at our knowledge, operando XANES spectroscopy to monitor the photoinduced changes in the spiropyran Zn complex.

2. Methods

Electronic absorption spectra and kinetic curves of the investigated compounds were recorded on a spectrophotometer (Agilent 8453 from Agilent Technologies) equipped with a thermostatic cell. The irradiation of solutions with filtered light was performed using a Xe arc lamp (66902 Arc Lamp Housing from Newport) equipped with a monochromator. The photon flux power was measured with a Newport power meter 2903-C. To compare measurements at different irradiation wavelengths a correction of the proportion of the absorbed light was adopted (see section S2 in SI for the details). The solutions for spectrophotometric investigations were prepared by mixing exact aliquots of standard $6 \cdot 10^{-4}$ M solutions of SPP and zinc perchlorate with subsequent dilution in 10 ml flasks. The solutions were allowed to equilibrate for 24 h under dark conditions for complete metal ion complexation. Acetone of the spectroscopic grade and zinc perchlorate (from Aldrich) were used to prepare solutions.

Zn K-edge XANES spectra were measured at Super-XAS beamline, Swiss Light Source. Incoming X-ray radiation from the bending magnet was monochromatized by Si(111) monochromator and focused by the toroidal mirror to 100x100 μm^2 spot size at the sample position. The proper amount of sample was dissolved in acetone to achieve 1 mM or 0.3 mM concentrations for static and photodynamic measurements correspondingly. Gear pump was used for circulation liquid through 500 μm nozzle to generate cylindrical liquid jet with 10 m/s flow speed. Nanosecond laser with fundamental frequency 532 nm, 150 kHz repetition rate and 100 mW power at sample position was used to excite solution. The laser was focused by cylindrical lenses to the 200×1500 μm^2 spot. For the alignment of X-ray with a laser beam, we used a pinhole. Details of the alignment procedure are described in section S1 of Supplementary Information. Both photo-accumulation under continuous illumination and pump-flow-probe

scheme described in work[34] were used. For the X-ray fluorescence detection, we used APD detector, triggered by the signal generator synchronously with the laser shutter.

The synthesis of the SPP**2** has been described earlier[35]. The SPP**1** has been obtained according to the analogous method[35] by condensation of the corresponding *3H*-indolium salts with benzothiazolyl substituted aldehyde. ^{1}H NMR spectra have been registered on a Varian Unity-300 (300 MHz) spectrometer using a $CDCl_3$ solution at 20°C. The signals assignment has been carried out with reference to the deuterosolvent (7.24 ppm). Elemental analysis was carried out using a KOVO CHN analyzer. Melting points were determined on a Boetius hot stage apparatus. High-resolution mass spectra were obtained from a TOF mass spectrometer with an ESI source (Bruker maXis). The instrument was operated in positive mode using an m/z range of 50-3000. The capillary voltage of the ion source was set at 4500 V. The nebulizer gas pressure was 0.4 bar, the drying gas flow was set to 4.0 L/min.

8-**(Benzo[*d*]thiazol-2-yl)-5',6-dichloro-1',3',3'-trimethylspiro[chromene-2,2'-indoline]** (SPP**1**). Yield 67%, m. p. 250-251 °C (heptane-toluene, 3:1). NMR ^{1}H, δ, ppm. (*J*, Hz): 11.28 (3H, s, 3-Me); 1.33 (3H, s, 3-Me); 2.70 (3H, s, 1-Me); 5.93 (1H, d, *J* = 10.3, 3'-H); 6.51 (1H, d, *J* = 8.2, 7-H); 6.94 (1H, d, *J* = 10.3, 4'-H); 7.13 (1H, d, *J* = 2.1, 4-H); 7.18 (1H, d, *J* = 2.6, 5'-H); 7.23 (1H, dd, *J* = 8.2, 2.1, 6-H); 7.32 (1H, ddd, *J* = 8.2, 7.1, 1.2, 6-H thiaz); 7.44 (1H, ddd, *J* = 8.3, 7.2, 1.3, 5-H thiaz); 7.64 (1H, ddd, *J* = 7.9, 1.3, 0.7, 7-H thiaz); 8.01 (1H, ddd, *J* = 8.2, 1.2, 0.7, 4-H thiaz); 8.41 (1H, d, *J* = 2.6, 7'-H). Calc d %: C 65.14; H 4.20; N 5.84. Found %: C 65.02; H 4.34; N 6.14. $C_{26}H_{20}Cl_2N_2OS$. HRMS (ESI+): m/z calcd. for $C_{26}H_{20}Cl_2N_2OS$ $(M+H)^+$: 479.0746, found: 479.0746.

Geometry optimization and Mulliken charge analysis were performed within B3LYP density functional level of the theory[36] using ADF-2017 program package[37, 38]. The largest available basis set was used which included quadruple-zeta basis with four polarization functions (QZ4P)[39]. Convergence criteria for the self-consistent calculation were set smaller 10^{-5} Hartree. The bonding energy was calculated as a difference between total energy and the energies of H_2O, acetone ligands and Zn^{2+} ion. Zn K-edge XANES spectra for DFT optimized structures were calculated by means of full-potential finite difference method, implemented in the FDMNES code[30]. The finite difference grid with 0.2 Å interpoint distance was constructed inside a sphere with 6 Å radius around absorbing Zn. Theoretical spectra were further convoluted to account for the corehole lifetime broadening and instrumental energy resolution (arctangent function was used to model the energy dependence of the Lorentzian width).

3. Results and discussion

3.1 Spectral and photochromic characteristics of the SPP ligands.

Variation of chelating substituents in the structure of spiropyran ligands is an effective way of modulating both chelating and photochromic properties. In this regard, we synthesized a new SPP**1** containing the benzothiazole substituent at position 8 of the pyran moiety. SPP**1** in solutions of both nonpolar and polar solvents appears as its SP form. The absorption spectrum of **1** in acetone is characterized by a structured long wavelength band with maxima at 355 (ε = 8860 $M^{-1}cm^{-1}$) and 370 (ε = 8000 $M^{-1}cm^{-1}$) nm. Like its benzoxazole containing analogue **2**, SPP**1** exhibits photochromic properties: UV light irradiation of its solution (λ_{irr} = 365 nm) leads to the intense coloration typical of photoinitiated formation of the merocyanine form. The long

wavelength absorption band of the merocyanine shows indeed a maximum at 648 nm (ε = 46000 $M^{-1}cm^{-1}$). After switching off the irradiation source a thermal back-reaction merocyanine → initial spirocyclic form is observed. The process is accompanied by a solution bleaching. The lifetime of the MC form is 25 s at 293 K. To estimate quantitatively the efficiency of the forward and reverse photochromic reactions a photokinetic method has been used. The method is based on the analysis of the kinetic curves obtained under successive steady-state irradiation of a solution of 1 with UV (λ_{irr} = 365 nm) and visible (λ_{irr} = 546 nm) light[35]. It has been established that the forward photoreaction quantum yield (QY) is 0.075 while the efficiency of the back photoprocess is two orders of magnitude lower ($4 \cdot 10^{-4}$). Comparing the obtained results with the data found for SPP**2** it can be concluded that substitution of the oxygen atom in the benzazole fragment with the sulphur one leads to a bathochromic shift of the absorption bands of the SP and MC forms as well as to the significant decrease of the efficiency of the reverse photochemical cyclization of the merocyanine into the spirocyclic isomer.

3.2 Static properties of the SPP**1**-Zn complex

As it has been recently shown 8-benzoxazole substituted spiropyrans interact in the dark with transition metal ions, particularly with zinc cations, producing intensely colored complexes[40]. Indeed SPP**1**, as well as its benzoxazole analogue **2**, interacts with zinc ions: upon addition of zinc perchlorate to a colorless SPP**1** or **2** solution in acetone the appearance of the intense red coloration has been observed. Color changes can be explained by the formation of the Zn-MC complex as shown in Scheme 1.

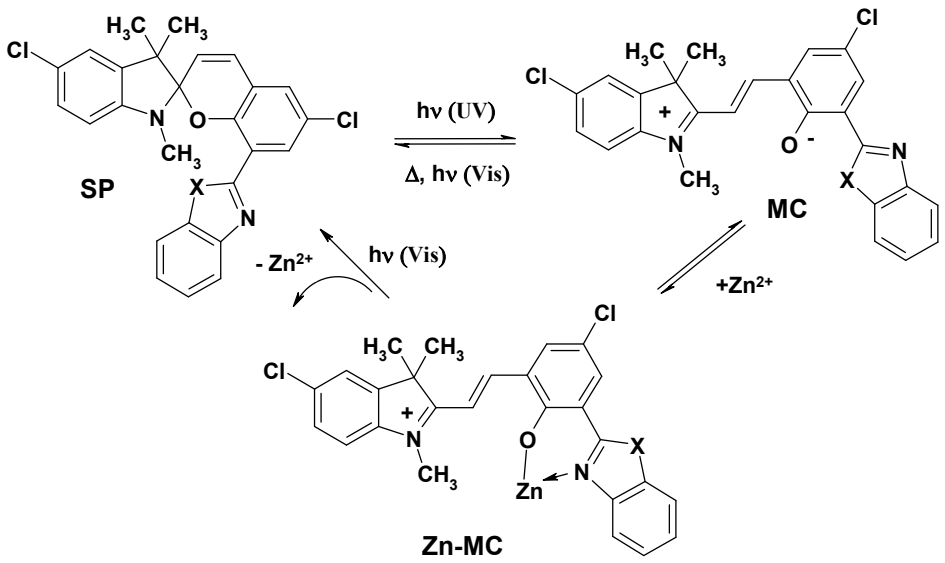

Scheme 1. Thermal and Photochemical Processes Accomplishing Interaction of SPP **1, 2** with Zn^{2+}. **1**: X = S, **2**: X = O

The formed SPP**1**-Zn complex shows a 1:1 stoichiometry and is characterized by a long wavelength absorption band with a maximum at 525 nm (ε = 32330 $M^{-1}cm^{-1}$). The stability constant determination for zinc complex of SPP**1** has been carried out by means of the UV/Vis spectroscopy according to the previously described procedure[40]. UV-vis spectra for SPP**1**-Zn complex for different Zn concentrations are shown in figure 1.

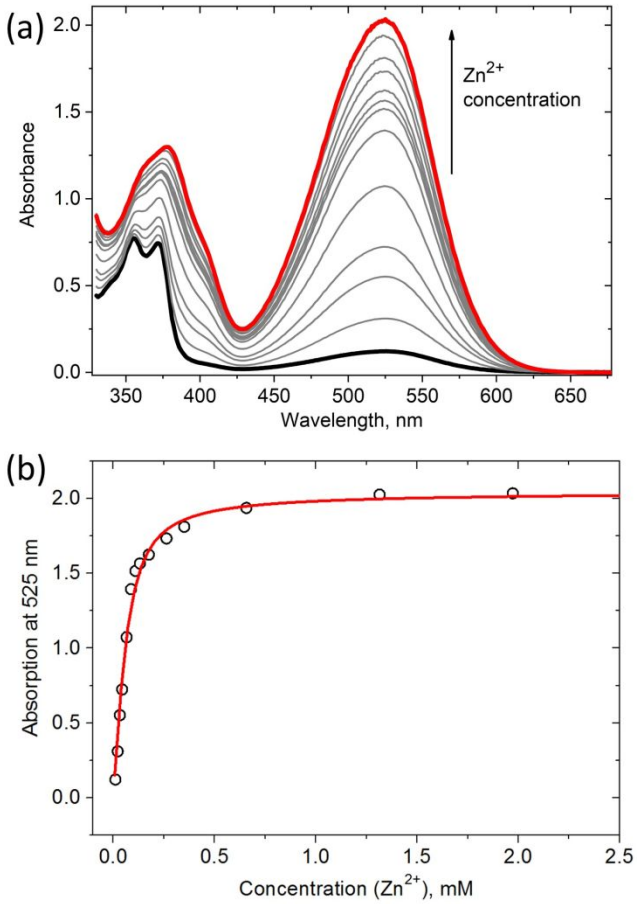

Figure 1. (a) UV-Vis (or electronic) absorption spectra of SPP**1** (C = $6.32 \cdot 10^{-5}$ M) as a function of $Zn(ClO_4)_2$ content from $6.98 \cdot 10^{-6}$ M to $1.26 \cdot 10^{-3}$ M (bottom and upper bold curves, respectively); (b) Dependence of the absorbance at the maximum of the SPP**1**-Zn complex absorption at 525 nm on $Zn(ClO_4)_2$ concentration (circles are the experimental data, solid line is the fit).

Stability constants were obtained from the fit of the absorption dependency on the Zn^{2+} concentration, shown in figure 1b. Dependence of the absorbance on the metal ion concentration was simulated in a model of 1:1 complex formation stoichiometry according to the procedure described in work[40]. Quantitative spectral characteristics of the complexes are listed in table 1. The complex formation is accompanied by a large hypsochromic shift of the absorption band

compared to the corresponding MC isomer. Noteworthy, the nature of the azole substituent in the position 8 affects the thermodynamic stability of complexes: upon transition from benzoxazole (SPP**2**) to benzothiazole (SPP**1**) slight stability decrease of the corresponded zinc complexes is observed (see table 1).

3.3 Photoinduced properties of the complex under continuous irradiation

The complexes with zinc ions exhibit fluorescence at λ>550 nm (fig.2) with a maximum at 640 nm and 655 nm for SPPs **1**, **2**, correspondingly, with fluorescence quantum yields of 0.191 and 0.188 (table 1).

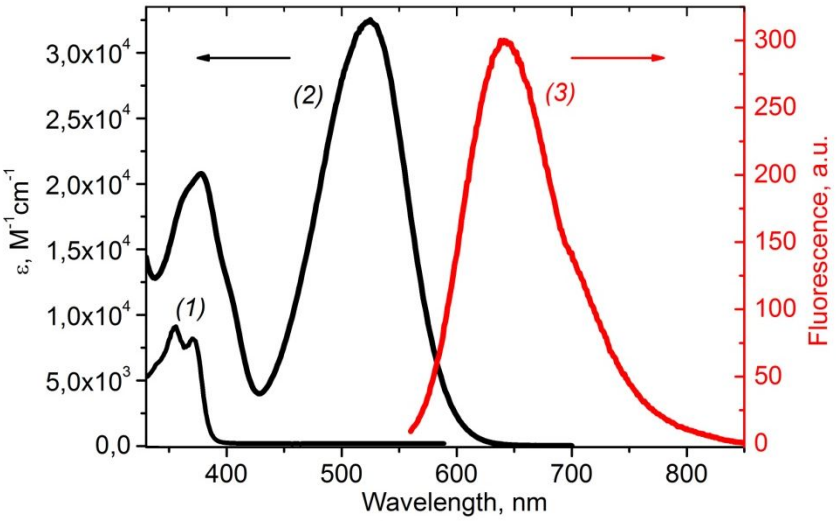

Figure 2. Absorption spectra of SPP**1** (*1*) and its Zn complex (2) in acetone. (3) Fluorescence emission spectrum of Zn complex.

Steady-state irradiation with visible light of a solution of spiropyran complexes with zinc ions into long wavelength absorption band region causes sharp discoloration. The absorption band of the complex disappears while initial SP form band is restored (figure 3). We recorded this process for the full spectrum of sunlight in the video in SI.

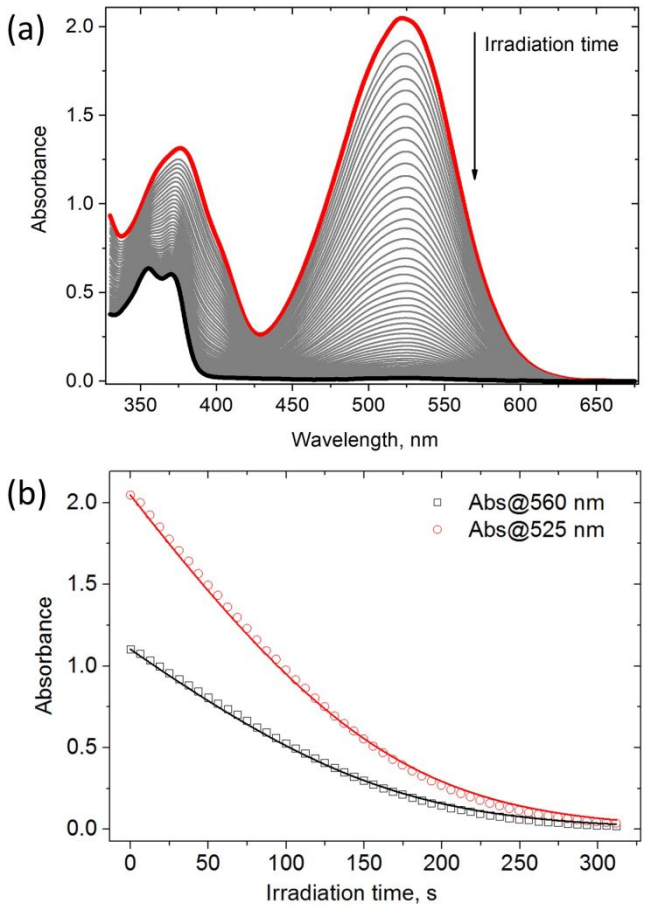

Figure 3. (a) Kinetics of the absorption spectra of a solution of SPP**1**-Zn complexes under 560 nm light irradiation, $I^{560} = 1.79 \cdot 10^{-6}$ mol·L^{-1}s^{-1}; (b) Dependence of the absorbance of the SPP**1**-Zn complex solution at the 525 nm (absorption maximum) and 560 nm (irradiation wavelength) on the irradiation time. Points are experimental results; lines are results of the kinetic modeling (see equation (1) and relative discussion).

Color recovery of the irradiated solution happens in the dark in several hours, corresponding to the time of complex formation after mixing of the initial spiropyran and Zn solutions. This is an indication that visible irradiation promotes complex dissociation. This effect provides a key

peculiarity of such type of compounds, particularly significant from the point of view of the application. Therefore, photoswitching between the colored complex and the colorless SP form of a ligand has been further quantitatively studied to determine the photoreaction quantum yield. Since the Zn complexes of **1** and **2** are characterized by a broad long-wave absorption band, the determination of the wavelength dependence of the quantum yield has been also carried out. The process of the photoinduced decomposition of the complex can be described by the equation (1)[40].

$$-d[\text{Zn-}\mathbf{MC}]/dt = I^0\Phi_r(1\text{-}10^{-\varepsilon'[\text{Zn-}\mathbf{MC}]l}) - k_\Delta\,(C_0\text{-}\,[\text{Zn-}\mathbf{MC}]) \qquad (1)$$

Where I^0 - incident light flux ($mol\cdot L^{-1}s^{-1}$), ε' - molar extinction coefficient of complex at the irradiation wavelength ($L\cdot mol^{-1}cm^{-1}$), l - optical path length for the incident light (cm), $A' = \varepsilon'[\text{Zn-}\mathbf{MC}]l$ optical density of solution at irradiation wavelength , C_0 – the complex concentration at t = 0. The current value of the complex concentration [Zn-**MC**] can be obtained from the solution absorption spectra recorded under irradiation with the help of Beer'law [**MB**] = $A_\lambda/\varepsilon_\lambda l$.

To get more insight into the photophysics of the metal complexes and to establish a general validly of the X-ray measurements reported in the following, we determined the dependence of the quantum yield on the irradiation wavelength. At this aim, the central wavelength of the monochromator after the Xe arc lamp was varied within the absorption band of the Zn-complex (from 450 nm to 570 nm). With respect to our previous experiments based on Hg lamp, now the spectral distribution of the irradiation source is essentially a continuum allowing an optimal spectral coverage.

To obtain kinetic curves the exact volume of a complex solution of the known concentration was irradiated by the monochromatized light. Series of photoinduced spectral changes similar to

ones shown in figure 3 were obtained for several wavelengths across the main absorption band of the complex. The solution absorption spectra were recorded at the 90° angle to the exciting light flux. The experimental photokinetic plots were modeled according to the equation (1) which was solved by numerical integration using the semi-explicit Runge-Kutta method[41, 42]. The residual error (*RE*) was estimated as:

$$RE = \frac{1}{N_p N_j} \sum_{p}^{N_p} \sum_{j}^{N_j} \left[A_{calc}(p,j) - A_{exp}(p,j) \right]^2 \quad (2)$$

where *p* is the index of the photokinetic curves and *j* is the index of the data points on each photokinetic curve. Numerical simulations were carried out with the simulation-adjustment program SA 3.3 (non-commercial software, Laboratoire des IMRCP, Université Paul Sabatier, Toulouse, France)[43].

As seen from fig. 3b, the experimental data are satisfactorily approximated within the used model. We found (see figures 4 and S3) that the efficiency of photoreaction is independent on the wavelength of the initiating radiation within the limits of the long wavelength absorption band. This fact can be explained either by the dominant presence in the solution of the one merocyanine isomer type or by several isomers with similar photoreaction yields (e.g. *TTT*, *TTC* and *CTC* isomers).

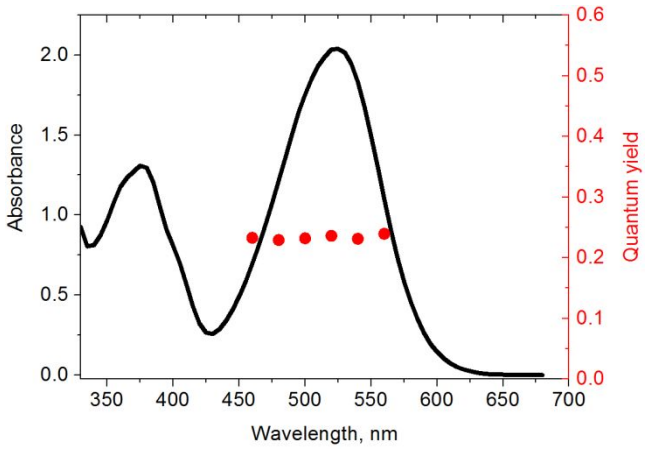

Figure 4. Dependence of the photoreaction quantum yield values of the SPP**1**-Zn complex on the irradiation wavelength (complex absorption spectrum is shown for clarity). The case of the SPP **2**-Zn complex is shown in fig.S3.

Table 1. Spectroscopic, Thermodynamic and Kinetic Properties of Zn Complexes of SPP **1**, **2**

SPP	$logK_1^{eff}$	Absorption		Fluorescence		Photoreaction QY (λ_{irr} = 546 nm)
		λ_{max}^{abs}, nm	$\varepsilon \cdot 10^{-4}$, $M^{-1} \cdot cm^{-1}$	λ_{max}^{fl}, nm	Φ_{fl}	Φ_r
1	4.53±0.01	525	3.23	640	0.191	0.236
2	5.29±0.01	523	3.80	655	0.188	0.212

We can address the structure of the irradiated complex by means of X-ray absorption spectroscopy. Figure 5b shows Zn K-edge XANES for the 1 mM Zn^{2+} ions in the solution before and after their reaction with ligand SPP**1**. The differences between two spectra are related to the shift of the absorption edge and decreasing of the intensity of the peaks A and C. The first fact can be attributed to the ligand substitution while the second one can be explained by the lower coordination number and higher disorder in the first shell. We performed DFT calculations to

obtain additional insight into Zn^{2+} coordination. The source of Zn^{2+} ions for the experiment was $Zn(ClO_4)_2(H_2O)_6$. After its dissolution in acetone, free Zn^{2+} ions will contain both water and acetone molecules in the first coordination shell. Bond energies for the whole set of complexes and their geometries are shown in section S6. When present, SPP**1** ligand substitutes several solvent molecules. Relaxed geometries and corresponding bonding energies for the complete set of $[Zn(C_3H_6O)_x(H_2O)_y]^{2+}$ and $[Zn(SPP\mathbf{1})(C_3H_6O)_x(H_2O)_y]^{2+}$ complexes are provided in section S6 of SI. We observed that bonding energies of SPP**1**-Zn complexes are lower by ~0.7 eV than those of free Zn^{2+} ions. This is consistent with experimentally observed complexation process. Furthermore, the most stable are the structures with higher coordination number among 4-, 5- and 6- coordinated Zn. The structures with the lowest energy are listed in Table 2 and shown in figure 5a. Calculations for Zn^{2+} ions predict the most stable model containing 4 acetone molecules and two water molecules in the first coordination shell and average Zn-O distance R_{Zn-O} 2.11 Å. Further coordination by SPP**1** results in the substitution of several solvent molecules by large SPP and average coordination number decreases. The most stable SPP**1**-Zn complex is that with formally 6-coordinated Zn^{2+} surrounded by four solvent molecules and SPP**1** ligand in its MC form. However, this model contains five bonds in the first coordination sphere of Zn^{2+} with an average length of 2.09 Å, while the sixth bond length equals 2.50 Å. First shell EXAFS analysis described in section S4 of SI indicates lower coordination number of Zn^{2+} in SPP**1**-Zn supporting results of DFT simulations.

Table 2. Bonding energies and Mulliken charge for the most stable structures of solvated Zn ion and SPP**1**-Zn complex. The values for $[Zn(H_2O)_6]^{2+}$ complex are shown for comparison. The data for other acetone and water stoichiometries are shown in table S2 of SI.

Complex	Bonding Energy, eV	Zn Mulliken Charge, electrons
$[Zn(H_2O)_6]^{2+}$	-6.64	+1.64
$[Zn(C_3H_6O)_4(H_2O)_2]^{2+}$	-6.80	+1.53
$[Zn(SPP\mathbf{1})(C_3H_6O)_2(H_2O)_2]^{2+}$	-7.50	+1.52

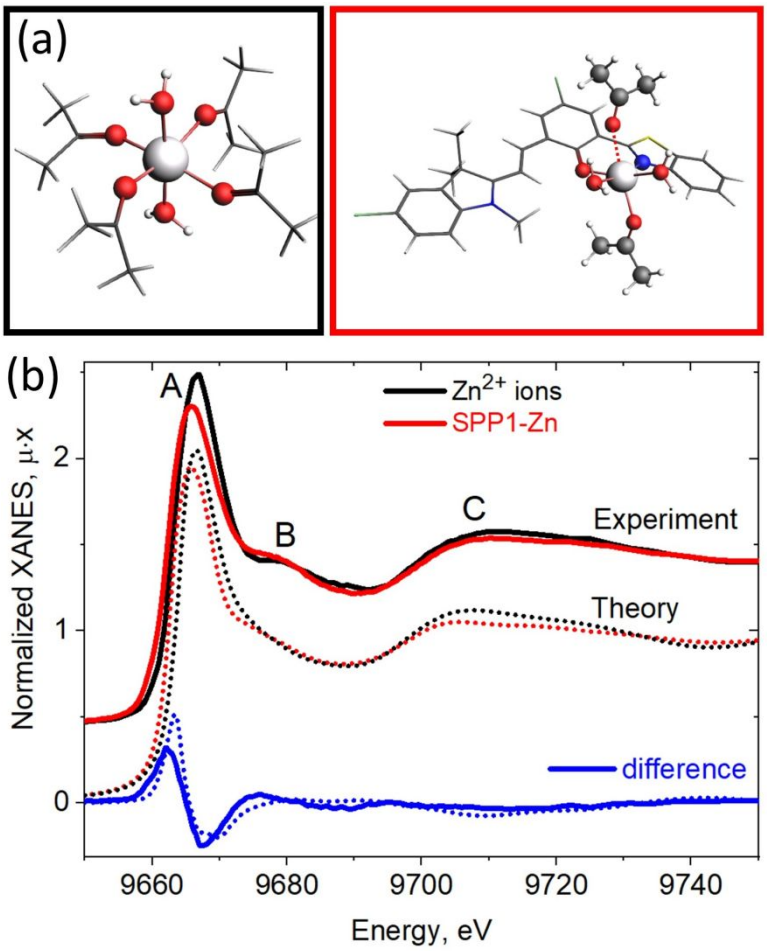

Figure 5. (a) Theoretical structural models with the lowest energies for the Zn^{2+} in acetone and SPP**1**-Zn complex. (b) Experimental Zn K-edge XANES spectra for the 1 mM solution of the $Zn(ClO_4)_2 \cdot 6H_2O$ in acetone before and after reaction with SPP**1** (upper solid curves) compared to the theoretical simulations for structures in panel (a).

The influence of the type of ligands in the first coordination shell on the position of the absorption edge is especially clear for the chlorine atoms. Liu et. al.[44] showed a variation of the Zn^{2+} K-edge XANES spectra for different concentration of NaCl in solution. Both the shape and position of absorption edge changed though formal oxidation state of Zn did not vary. In the present study position of the Zn absorption edge shifted to lower energy after fresh Zn^{2+} solution in acetone was equilibrated with time. Figure S4 in SI shows 0.4 eV negative energy shift after 20 minutes of acquisition, compared to the initial spectrum. This fact can be explained by the substitution of the initial water molecules by the acetone ones in the solvation shell. Variation of the Zn charge upon such replacement is proved by Mulliken charge analysis shown in Table 2. Mulliken charge for free Zn^{2+} decreased by 0.11 electrons when four water molecules were detached from the Zn^{2+} ion. Further decrease of the calculated charge for Zn ion is observed upon coordination by MC.

The energies of five- and six-coordinated SPP**1**-Zn complexes with different combinations of water and acetone molecules in the solvation shell suggest the thermal equilibrium between several configurations. Figure 6 shows XANES spectra for all DFT optimized models reviewed in table S2 of SI. Giachini et.al.[45] have studied theoretically and experimentally Zn K-edge XANES for the metalloproteins as a function of Zn^{2+} coordination number. They found that the white line intensity (peak A reported in our case at figures 6 and 5b) is proportional to the Zn coordination number and whole XANES spectrum could be used to evaluate binding motifs of the metalloprotein active center. From our calculations in figure 6 we observe a similar tendency. The intensity of feature A increases along with Zn coordination number. Peaks B-D show a clear dependence on the coordination number. Peak B is larger for lower coordination numbers. The same is true for the relative intensity of peaks C and D – μ_D/μ_C.

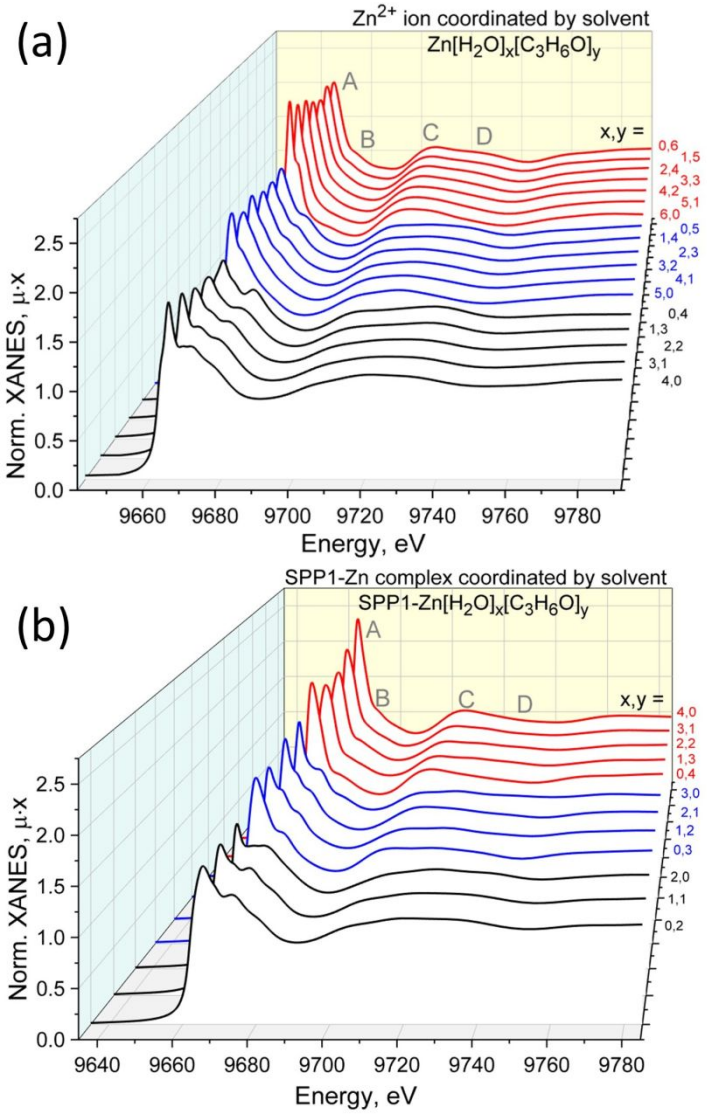

Figure 6. Theoretical Zn K-edge XANES spectra for the series of Zn^{2+} ions and SPP**1**-Zn complexes, coordinated by solvent molecules. The total number of ligands in the first coordination shell of Zn varied from 4 to 6 with a different stoichiometry of water and acetone molecules (see Table S2 in SI for details). The color code is used to separate structures with different coordination numbers: black is used for the 4-coordinated complexes, blue – for the 5-coordinated and red for the 6-coordinated complexes (note that for SPP**1**-Zn complex SPP**1** ligand provides two atoms for coordination).

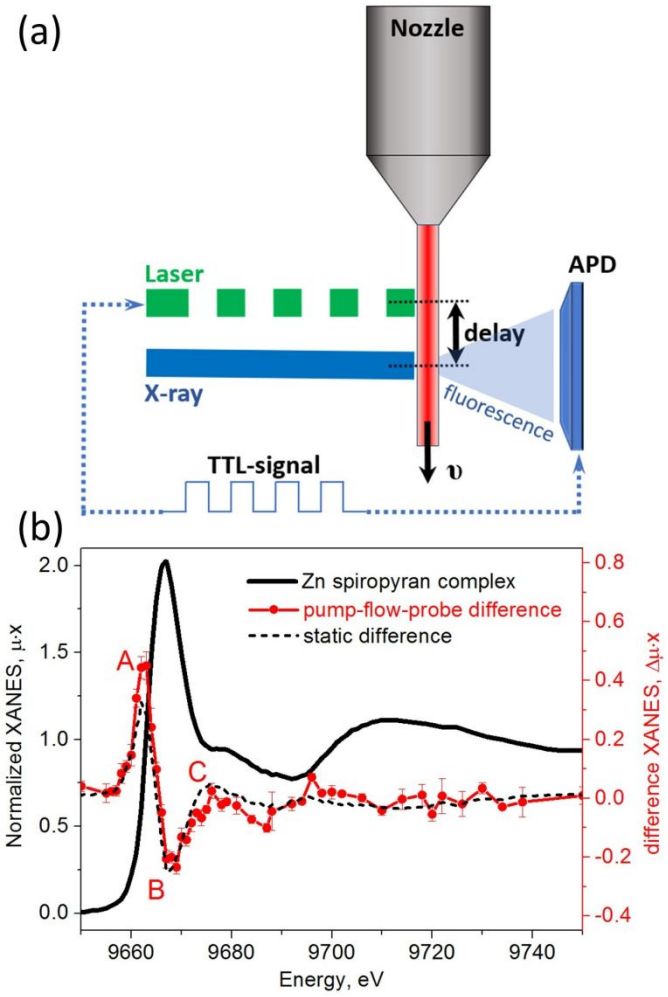

Figure 7. (a) Scheme of the pump-flow-probe experiment. (b) Transient XANES spectrum (red symbols) obtained from the Laser ON/Laser OFF switches synchronized with the X-ray data acquisition system. The transient signal is compared to the static difference shown in figure 5b.

Figure 7a shows a scheme of the sample irradiation and simultaneous acquisition of XANES spectra. A focused laser beam with 200 μm vertical height and 1500 μm horizontal width irradiated the cylindrical jet. For every energy point we acquired X-ray fluorescence signal from the point 200 μm below the laser beam center with laser ON and laser OFF. Size of the X-ray beam was 100x100 μm^2. Jet flow speed was set 10 m/s thus delay between laser irradiation and X-ray fluorescence acquisition was equal to 20±5 μs. Figure 7b shows the difference signal

between laser ON and OFF spectra, accumulated over 3 hours. Each energy point was measured 6 times and measurements were repeated several times for different laser power and jet thickness providing a reproducible signal. To prevent accumulation of the photoproducts we used 1 L of the 0.3 mM sample solution in the circulation system. If the sample volume was smaller than 200 ml the photo-accumulated species became prominent (see an analysis of spectra in figures S6 and S7 of SI, acquired for 80 ml of 1 mM SPP**2**-Zn complex).

We compare the pump-flow-probe transient signal with the static difference shown with the dashed line in figure 7b. Both difference curves match in the energy positions of peaks A, B, C, and their relative intensities. However, the difference obtained in the pump-flow-probe regime has the slightly higher intensity of the peak A, which can be explained by the differences in the 1st coordination shell of the equilibrated Zn^{2+} ions and Zn^{2+} produced shortly after photoreaction. Within the 20 μs timescale we expect that bond Zn-O(SPP) is broken (see Scheme 1) while some fraction of Zn ions can still retain Zn-N(SPP) bond. This fraction of Zn ions is thus coordinated by the spirocyclic form of SPP**1** ligand and has lower than 6 coordination number due to steric effects.

Conclusions

Formation and photoreaction of Zn complexes with MC form of 6-benzazole substituted SPP **1, 2** were studied by means of operando UV-vis and Zn K-edge XAS spectroscopies. Complexes are characterized by maximum absorption at 523 and 525 nm with a molar absorption coefficient of 3.2 – 3.8 $\cdot 10^4$ $M^{-1}cm^{-1}$ and binding constants 4.53 and 5.29 (log units), respectively. Irradiation of complex solutions with visible light induces photo discoloration with quantum yield 21.2 and 23.6 %. For the first time we showed that photoreaction induces changes in the Zn local atomic structure but not only ligand isomerization. We have achieved 20 μs time resolution in the pump-

flow-probe scheme and showed that after this time Zn ions are released from the complex and present as $[Zn(C_3H_6O)_x(H_2O)_{6-x}]^{2+}$ complexes. Within this timescale, the small fraction of Zn^{2+} can exist in the complex with a spirocyclic isomer of the ligand. This work opens new perspectives of using XAS in the operando diagnostics of metal complexes of photoswitchable ligands.

Supporting Information. Details of the alignment procedure, analysis of the dependence of the photoreaction quantum yield on incident wavelength, dissociation of the aquated $Zn(ClO_4)_2 \cdot 6H_2O$ salt in acetone, accumulation of the photoproduct for small circulation volumes. EXAFS analysis of the solvated Zn^{2+} and SPP**1**-Zn complex. Binding energies and coordinates for DFT optimized structures.

AUTHOR INFORMATION

Corresponding Author

avchernyshev@sfedu.ru, guda@sfedu.ru

Author Contributions

The manuscript was written through the contributions of all authors. All authors have given approval to the final version of the manuscript

ACKNOWLEDGEMENT

This work was financially supported by the Ministry of Education and Science of the Russian Federation within the framework of the State Assignment for Research (project No. 4.9645.2017/8.9). We thank the Swiss Light Source for providing beam time at the SuperXAS beamline.

REFERENCES

1. Guglielmetti, R. 4n+2 Systems: Spiropyrans. In *Photochromism: molecules and systems;* Dürr, H., Bouas-Laurent, H., Eds.; Elsevier: Amsterdam, 1990; Ch.8, pp 314-466.

2. Bertelson, R. C. Spiropyrans. In *Organic Photochromic and thermochromic compounds. Topics in Applied Chemistry;* Crano, J. C.; Guglielmetti R. J. Eds.; Plenum Press: New York, 1999; Vol. 1, pp 11-83.

3. Minkin, VI. Photo-, Thermo-, Solvato-, and Electrochromic Spiroheterocyclic Compounds. *Chem. Rev.* **2004**, *104*, 2751-2776.

4. Kubinyi, M.; Varga, O.; Baranyai, P.; Kállay, M.; Mizsei, R.; Tárkányi, G.; Vidóczy, T. Metal Complexes of the Merocyanine Form of Nitrobenzospyran: Structure, Optical Spectra, Stability. *J. Mol. Struct.* **2011**, *1000*, 77-84.

5. Wojtyk, J.C; Kazmaier, P. Effects of Metal Ion Complexation on the Spiropyran–Merocyanine Interconversion: Development of a Thermally Stable Photo-switch. *Chem. Commun.* **1998**, 1703-1704.

6. Inouye, M. Artificial Signaling Receptors for Biologically Important Chemical Species. *Coord. Chem. Rev.* **1996,** *148*, 265-283.

7. Paramonov, S.V.; Lokshin, V.; Fedorova, O.A. Spiropyran, Chromene or Spirooxazine Ligands: Insights into Mutual Relations Between Complexing and Photochromic Properties. *J. Photochem. Photobiol., C* **2011**, *12,* 209–236.

8. Qin, M.; Huang, Yu.; Li, F.; Song, Y. Photochromic Sensors: a Versatile Approach for Recognition and Discrimination. *J. Mater. Chem. C.* **2015**, 9265-9275.

9. Sahoo, P. R.; Prakash, K.; Kumar, S. Light Controlled Receptors for Heavy Metal Ions. *Coord. Chem. Rev.* **2018**, *357*, 18–49.

10. Heng, S.; Mak, A.M.; Stubing, D.B.; Monro, T.M.; Abell, A.D. Dual Sensor for Cd(II) and Ca(II): Selective Nanoliter-Scale Sensing of Metal Ions. *Anal. Chem.* **2014**, *86*, 3268−3272.

11. Byrne, R.; Ventura, C.; Lopez, F.B.; Walther, A.; Heise, A.; Diamond, D. Characterisation and Analytical Potential of a Photo-responsive Polymeric Material Based on Spiropyran. *Biosens. Bioelectron.* **2010**, *26*, 1392–1398.

12. Heng, S.; McDevitt, C.A.; Kostecki, R.; Morey, J.R.; Eijkelkamp, B.A.; Ebendorff-Heidepriem, H.; Monro, T.M.; Abell, A.D. Microstructured Optical Fiber-based Biosensors: Reversible and Nanoliter-Scale Measurement of Zinc Ions. *ACS Appl. Mater. Interfaces* **2016**, *8*, 12727−12732.

13. Genovese, M. E.; Caputo, G.; Nanni, G.; Setti, C.; Bustreo, M.; Perotto, G.; Athanassiou, A.; Fragouli, D. Light Responsive Silk Nanofibers: An Optochemical Platform for Environmental Applications. *ACS Appl. Mater. Interfaces* **2017**, *9*, 40707−40715.

14. Goswami, S.; Aich, K.; Das, S.; Kumar Das, A.; Sarkar, D.; Panja, S.; Kumar Mondalb, T. Mukhopadhyay, S. A Red Fluorescence 'Off–On' Molecular Switch for Selective Detection of Al^{3+}, Fe^{3+} and Cr^{3+}: Experimental and Theoretical Studies Along with Living Cell Imaging. *Chem. Commun.* **2013**, *49*, 10739-10741.

15. Rivera-Fuentes, P.; Lippard, S.J. SpiroZin1: A Reversible and pH-Insensitive, Reaction-Based, Red-Fluorescent Probe for Imaging Biological Mobile Zinc. *ChemMedChem.* **2014**, *9*, 1238 -1243.

16. Rivera-Fuentes, P.; Wrobel, A. T.; Zastrow, M. L.; Khan, M.; Georgiou, J.; Luyben, T. T.; Roder, J. C.; Okamoto, K.; Lippard, S. J. A Far-red Emitting Probe for Unambiguous Detection of Mobile Zinc in Acidic Vesicles and Deep Tissue. *Chem. Sci.* **2015**, *6*, 1944–1948.

17. Heng, S.; Reineck, P.; Vidanapathirana, A. K.; Pullen, B. J.; Drumm, D. W.; Ritter, L. J.; Schwarz, N.; Bonder, C. S.; Psaltis, P. J.; Thompson, J. G.; et al. Rationally Designed Probe for Reversible Sensing of Zinc and Application in Cells. *ACS Omega* **2017**, *2*, 6201−6210.

18. Li, Y.; Zhao, Y.; Chan, W.; Wang, Y.; You, Q.; Liu, C.; Zheng, J.; Li, J.; Yang, S.; Yang, R. Selective Tracking of Lysosomal Cu^{2+} Ions Using Simultaneous Target- and Location-Activated Fluorescent Nanoprobes. *Anal. Chem.* **2015**, *87*, 584−591.

19. Champagne, B.; Plaquet, A.; Pozzo, J.-L.; Rodriguez, V.; Castet, F. Nonlinear Optical Molecular Switches as Selective Cation Sensors. *J. Am. Chem. Soc.* **2012**, *134*, 8101−8103.

20. Minkin, V. I.; Starikov, A. G.; Starikova, A. A. Light-controlled Spin-State-Switching Rearrangements of Transition Metal Complexes with Photochromic Ligands. *Pure Appl. Chem.* **2017**, *89*, 985–1005.

21. Görner, H.; Chibisov, A. K. Complexes of Spiropyran-Derived Merocyanines with Metal Ions. Thermally Activated and Light-Induced Processes. *J. Chem. Soc., Faraday Trans.* **1998**, *94*, 2557-2564.

22. Selvanathan, P.; Huang, G.; Guizouarn, T.; Roisnel, T.; Fernandez-Garcia, G.; Totti, F.; Le Guennic, B.; Calvez, G.; Bernot, K.; Norel, L.; et al. Highly Axial Magnetic Anisotropy in a N_3O_5 Dysprosium(III) Coordination Environment Generated by a Merocyanine Ligand. *Chem. Eur. J.* **2016**, *22*, 15222 – 15226.

23. Selvanathan, P.; Dorcet, V.; Roisnel, T.; Bernot, K.;.Huang, G.; Le Guennic, B.; Norel, L.; Rigaut, S. *Trans* to *Cis* Photo-isomerization in Merocyanine Dysprosium and Yttrium Complexes. *Dalton Trans.* **2018**, *47*, 4139–4148.

24. Tu, C.; Louie, A. Y. Photochromically-controlled, Reversibly-activated MRI and Optical Contrast Agent. *Chem. Commun.* **2007**, 1331–1333.

25. Tu, C.; Osborne, E. A.; Louie, A. Y. Synthesis and Characterization of a Redox- and Light-Sensitive MRI Contrast Agent. *Tetrahedron* **2009**, *65*, 1241–1246.

26. Collins, G.E.; Choi, L.-S.; Ewing, K.J.; Michelet, V.; Bowen, C.M.; Winkler, J.D. Photoinduced Switching of Metal Complexation by Quinolinospiropyranindolines in Polar Solvents. *Chem. Commun*. **1999**, 321–322.

27. Smolentsev, G.; Sundström, V. Time-resolved X-ray Absorption Spectroscopy for the Study of Molecular Systems Relevant for Artificial Photosynthesis. *Coord. Chem. Rev.* **2015**, *304-305,* 117-132.

28. D'Angelo, P.; Migliorati, V. Solvation Structure of Zn^{2+} and Cu^{2+} Ions in Acetonitrile: A Combined EXAFS and XANES Study. *J. Phys. Chem. B.* **2015**, *119*, 4061–4067.

29. Smolentsev, G.; Soldatov, A. Quantitative Local Structure Refinement from XANES: Multi-dimensional Interpolation Approach. *J. Synchrotron Rad.* **2006**, *13*, 19-29.

30. Guda, S. A.; Guda, A. A.; Soldatov, M. A.; Lomachenko, K. A.; Bugaev, A. L.; Lamberti, C.; Gawelda, W.; Bressler, C.; Smolentsev, G.; Soldatov, A. V.; et al. Optimized Finite Difference Method for the Full-Potential XANES Simulations: Application to Molecular Adsorption Geometries in MOFs and Metal-Ligand Intersystem Crossing Transients. *J. Chem. Theory Comput.* **2015**, *11*, 4512–4521.

31. Guda, A.A.; Guda, S. A.; Soldatov, M. A.; Lomachenko, K. A.; Bugaev, A. L.; Lamberti, C.; Gawelda, W.; Bressler, C.; Smolentsev, G.; Soldatov, A. V.; et al. Finite Difference Method Accelerated with Sparse Solvers for Structural Analysis of the Metal-Organic Complexes. *J. Phys.: Conf. Ser.* **2016**, *712*, 012004.

32. Smolentsev, G.; Guda, A. A.; Janousch, M.; Frieh, C.; Jud, G.; Zamponi, F.; Chavarot-Kerlidou, M.; Artero, V.; van Bokhoven, J. A.; Nachtegaal, M. X-ray Absorption Spectroscopy with Time-Tagged Photon Counting: Application to Study the Structure of a Co(I) Intermediate of H_2 Evolving Photo-Catalyst. *Faraday Discuss.* **2014**, *171*, 259-273.

33. Moonshiram, D.; Guda, A.; Kohler, L.; Picon, A.; Guda, S.; Stefan Lehmann, C.; Zhang, X.; Southworth, S. H.; Mulfort, K. L. Mechanistic Evaluation of a Nickel Proton Reduction Catalyst Using Time-Resolved X-ray Absorption Spectroscopy. *J. Phys. Chem. C* **2016**, *120*, 20049–20057.

34. Smolentsev, G.; Guda, A.; Zhang, X.; Haldrup, K.; Andreiadis, E. S.; Chavarot-Kerlidou, M.; Canton, S. E.; Nachtegaal, M.; Artero, V.; Sundström, V. Pump-Flow-Probe X-ray Absorption Spectroscopy as a Tool for Studying Intermediate States of Photocatalytic Systems. *J. Phys. Chem. C* **2013**, *117*, 17367–17375.

35. Rostovtseva, I.A.; Solov'eva, E. V.; Chernyshev, A. V.; Voloshin, N. A.; Trofimova, N. S.; Metelitsa, A. V. Photo- and Thermochromic Spiropyrans 43. Spectral Kinetic Study of New Benzoxazolyl-substituted Spirobenzopyrans. *Chem. Heterocycl. Comp.* **2015**, *51*, 223 - 228.

36. Reiher, M.; Salomon, O.; Hess, B. A. Reparameterization of Hybrid Functionals Based on Energy Differences of States of Different Multiplicity. *Theor. Chem. Acc*. **2001**, *107*, 48-55.

37. te Velde, G.; Bickelhaupt, F. M.; Baerends, E. J.; Fonseca Guerra, C.; van Gisbergen, S. J. A.; Snijders, J. G.; Ziegler, T. Chemistry with ADF. *J. Comput. Chem.* **2001**, *22*, 931-967.

38. Guerra, C. F.; Snijders, J. G.; te Velde, G.; Baerends, E. J. Towards an Order-N DFT Method. *Theor. Chem. Acc.* **1998**, *99*, 391-403.

39. Van Lenthe E.; Baerends, E. J. Optimized Slater-type Basis Sets for the Eements 1–118. *J. Comput. Chem.* **2003**, *24*, 1142-1156.

40. Chernyshev, A.V.; Metelitsa, A .V.; Rostovtseva, I.A.; Voloshin, N. A.; Solov'eva, E.V.; Gaeva, E.B.; Minkin, V.I. Chromogenic Systems Based on 8-(1,3-Benzoxazol-2-yl) Substituted Spirobenzopyrans Undergoing Ion Modulated Photochromic Rearrangements. *J. Photochem. Photobiol., A* **2018**, *360*, 174-180.

41. Kaps, K.; Rentrop, P. Application of a Variable-order Semi-implicit Runge-Kutta Method to Chemical Models. *Comput. Chem. Eng.* **1984**, *8*, 393-396.

42. Deniel, M. H.; Lavabre, D.; Micheau, J. C. Photokinetics under Continuous Irradiation. In *Organic Photochromic and Thermochromic Compounds. Topics in Applied Chemistry*; Crano, J. C., Guglielmetti R. J., Eds.; Plenum Press: New-York, 1999; Vol. 2, pp 167-209.

43. For more details: http://cinet.chim.pagesperso-orange.fr/index.html (accessed December 22, 2018)

44. Liu, W.; Etschmann, B.; Foran, G.; Shelley, M.; Brugger, J. Deriving Formation Constants for Aqueous Metal Complexes from XANES Spectra: Zn^{2+} and Fe^{2+} Chloride Complexes in Hypersaline Solutions. *Am. Mineral.* **2007**, *92*, 761-770.

45. Giachini, L.; Veronesi, G.; Francia, F.; Venturoli, G.; Boscherini, F. Synergic Approach to XAFS Analysis for the Identification of Most Probable Binding Motifs for Mononuclear Zinc Sites in Metalloproteins. *J. Synchrotron Rad.* **2010**, *17*, 41-52.

TOC graphic

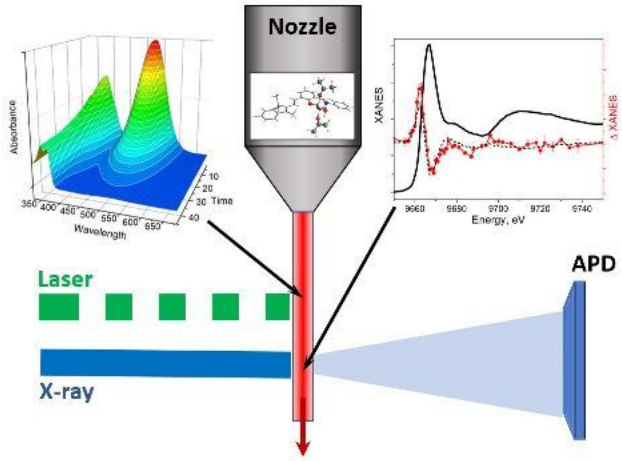
Nozzle
Absorbance
Wavelength
Time
XANES
Energy, eV
Laser
X-ray
APD